https://doi.org/10.1016/j.ymssp.2019.106312

Mid-to-high Frequency Piecewise Modelling of an Acoustic System with Varying Coupling Strength

Zhongyu HU[1], Laurent MAXIT[2] and Li CHENG[1]

[1]Department of Mechanical Engineering, The Hong Kong Polytechnic University, Hung Hom, Kowloon, Hong Kong, China

[2]Laboratoire Vibrations Acoustique, INSA Lyon, 25 bis, avenue Jean Capelle, 69621 Villeurbanne Cedex, France

*Corresponding author: li.cheng@polyu.edu.hk

Abstract

Mid-to-high frequency vibro-acoustic modelling has always been a challenging topic. Previous study shows the promise of a piecewise calculation scheme based on the Condensed Transfer Function (CTF) approach in a frequency range where the modal overlap factor roughly exceeds one. The piecewise scheme has shown its capability in terms of balancing the accuracy, efficiency and the wealth of information for the modeling of lightly coupled vibroacoustic systems. This paper extends the method beyond the weak-coupling assumption. A coupling strength factor is first proposed to quantify and adjust the coupling strength between two sub-systems. Two mutually connected sub-cavities are then used as an example to validate the piecewise scheme in relation to the changes in the coupling strength level, as well as the variations in the coupling strength factor itself. The effect of the coupling strength on the computational error of the piecewise scheme is systematically studied. Finally, the applicability of the piecewise calculation scheme is experimentally validated.

Key Words: *Mid-to-high frequency*; *Vibro-acoustic system*; *Substructure method*

Highlights:

- *A mid-to-high frequency vibro-acoustic modelling method is presented.*
- *A method for quantifying the coupling strength between two surface coupled systems is proposed.*
- *The accuracy and efficiency of the proposed modelling method for strongly coupled systems are demonstrated.*
- *The method is experimentally validated.*

1. Introduction

Numerical methods for predicting the acoustic responses of structures have been attracting intensive research interests for decades. In the low frequency range, Finite Element Method (FEM) and Boundary Element Method (BEM) are the two most powerful and popular tools [1, 2]. However, they become cumbersome when the target frequency increases to reach the so-called mid-to-high frequency range because of the significant increase in the required Degrees of Freedom (DoF), roughly linearly for the FEM and quadratically for the BEM. This motivated the long-lasting effort in the acoustic community to explore more efficient modelling approaches, as reviewed in Ref. [3].

Among existing methods, a typical one is the hybrid deterministic-statistical approach [4-7], which partitions the whole system into two types of components/sub-systems based on their deformation wavelengths, with long wavelength ones modelled deterministically by FEM or Wave Based Method (WBM) and the short ones by the Statistical Energy Analysis (SEA). However, confined by the underlying assumptions of the SEA, detailed descriptions of the statistical sub-systems responses are unavailable. Another type of approach can be categorized as sub-structuring methods, exemplified by the model reduction methods [8-10] and mobility methods [11-13]. Sub-structuring methods enable more detailed description of the short wavelength sub-systems than hybrid methods do. One of the representative mobility methods is the Patch Transfer Function (PTF) method, applicable to either structural-acoustic problems [12] and pure acoustic problems [13]. The PTF method was further generalized to the so-called Condensed Transfer Function (CTF) method which allows the transfer functions, also named condensation functions (CF), over the interface to be any orthonormal set like complex exponential functions or Chebyshev polynomials.

Using the full set of CFs, the effectiveness of the CTF method has been shown by investigating a submerged shell structure with internal line-coupled non-axisymmetric substructures [14].

One of the important developments on the CTF-based method is the previous attempt to increase its upper frequency limit without compromising its computational efficiency and its ability in providing detailed description of the physical system. Using a plate-cavity configuration, a piecewise calculation scheme was proposed for the mid-to-high frequency modelling [3]. By capitalizing on the wavy feature of the complex exponential functions as CFs, the piecewise calculation scheme allows the description of the dynamic behavior of the coupling interface by using a truncated sub-set of the full CF series for any given frequency band in the mid-to-high frequency range (starting from a frequency with a modal overlap factor roughly equal to one). As a consequence, the size of the system matrix to be solved becomes smaller, leading to a reduction of the computational cost and an increase in the frequency outreach. The computational efficiency of the method was demonstrated using a plate-cavity system in air. Despite the relevance of the configuration for many engineering applications [15-19], the system is considered as a typical weak coupling case [11]. The so-called weak coupling assumption applies to either a structural-acoustic system or a pure acoustic system composed of multiple sub-cavities. For the former, the fluid-loading effect on a mechanically excited structure is considered to be weak and negligible; for the latter, the acoustic response of an acoustically excited sub-cavity remains essentially the same no matter whether the connecting interface with its adjacent acoustic neighbor is open or closed as a rigid wall.

Therefore, examining the applicability of the piecewise calculation scheme in the context of increasing coupling strength is required. This, however, brings up two

challenging issues that the present work attempts to address and contribute to the existing knowledge. The first one, which is of general relevance, is to establish a metric to quantify the coupling strength level in a coupled system. Along the same line of thinking, a very useful coupling strength quantification method was proposed earlier [11], which applies to two coupled single DoF sub-systems. For two continuous sub-systems, the coupling coefficient in traditional modal theory can quantify the spatial matching level between two modes of the uncoupled sub-systems [20]. However, it does not reflect the frequency matching of these modes whereas it is known to be an important parameter of the energy exchanged between two coupled modes. Therefore, a more general assessment method depending also on the physical properties and the frequency characteristics is needed, especially under the context of the mid-to-high frequency. The second one, more specific to the CTF method itself, concerns the assessment of its applicability and the accuracy in dealing with cases when the coupling becomes stronger. It is well accepted that the energy flow between a weakly coupled system is substantially less than the energy dissipated within each subsystem [21], so that the assumptions and simplifications made under the weak coupling conditions might become invalid in the strong coupling cases. More specifically, the underlying assumption of the piecewise calculation scheme is that the energy is only concentrated in a few dominated terms, which deserves a re-examination and assessment when energy exchange between sub-systems becomes more complex with an increasing coupling strength. Therefore, whether and to what extent the piecewise scheme is still applicable under various coupling strength levels remains unknown. This forms the main motivation of the present work.

In this paper, the piecewise scheme is systematically scrutinized under different coupling strength levels. In Section 2, the CTF method and the piecewise scheme are

briefly recalled, based on which a coupling strength factor is defined to quantify the coupling strength between two sub-systems. A cavity composed of two mutually-connected chambers is then selected to conduct the analyses, whose coupling strength is tactically adjusted through tuning the geometrical parameters based on the proposed coupling strength factor. The piecewise calculation scheme is then examined in Section 3. Computational errors are analyzed with respect to different coupling strength levels, leading to the establishment of a relationship between them. Finally, experimental validations are carried out in Section 4 before conclusions are summarized in Section 5. Similar analyses on a structure-acoustic system are briefly presented in Appendix for reference.

2. Theoretical Analyses

For the sake of completeness, this section briefly recalls the CTF method and the piecewise calculation scheme. Then, a coupling strength factor is defined to quantify the coupling strength level between two sub-systems under the CTF framework. As an example, the theory is built upon an acoustic cavity system, although a structure-cavity system can also be treated in a similar way, as briefed in Appendix. Finally, the correlation between the coupling strength and the proposed coupling strength factor is validated.

2.1 CTF method and piecewise calculation scheme

2.1.1 CTF method

Consider a system composed of two sub-systems coupled over an interface Γ as shown in Fig. 1, in which the left one is either structural or acoustical, being excited

and noted as the main sub-system, and the right one is acoustical, noted as the attached sub-system,.

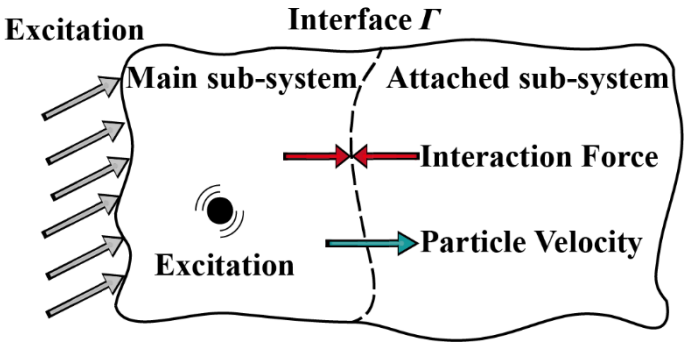

Figure 1 2D illustration of a system composed of two sub-systems that are coupled through an interface.

To illustrate the method, the case involving two acoustically coupled sub-cavities are used. To simplify the analyses process, the whole system is assumed to be coordinate separable so that the physical quantities, such as velocities or forces, on Γ can be described as $f(x,y)$. Then, a set of $N_x \times N_y$ orthonormal functions $\{\varphi_{rs}\}_{1\le r\le N_x, 1\le s\le N_y}$, referred to as *Condensation Functions* (CFs), is employed to approximate the velocities and the forces on Γ. For each acoustic sub-system, the condensed impedance $Z_{kl,rs}$ is defined by imposing a prescribed velocity $U(x,y) = \varphi_r(x)\varphi_s(y)$ on Γ as:

$$Z_{kl,rs} = \frac{<\bar{P}_{rs}, \varphi_{kl}>}{<U, \varphi_{rs}>} =< \bar{P}_{rs}, \varphi_{kl} >, \tag{1}$$

where $\bar{P}_{rs}$ is the blocked pressure on Γ when the subsystem is subjected to $U(x,y)$ and $<f, g>$ is a scalar product defined as $\int_\Omega f(x,y)g^*(x,y)dS$ with g^* being the complex conjugate of g. Then the normal velocity U^α and the normal pressure distribution P^α on Γ for each subsystem can be decomposed as:

$$\begin{cases} U^{\alpha}(x,y) = \sum_{r,s} u_{rs}^{\alpha} \varphi_r(x) \varphi_s(y) \\ P^{\alpha}(x,y) = \sum_{r,s} p_{rs}^{\alpha} \varphi_r(x) \varphi_s(y) \end{cases}, \tag{2}$$

where u_{rs}^{α} and p_{rs}^{α} are the amplitudes of the normal velocity and the normal pressure distribution with respect to the condensation function φ_{rs} for each uncoupled subsystem, with α=1 and α=2 referring to the main sub-cavity and the attached sub-cavity, respectively. On the other hand, the velocity continuity and force equilibrium over Γ between the two sub-systems give

$$\begin{cases} U^1 = U^2 \\ P^1 = -P^2 \end{cases}. \tag{3}$$

Then multiplying both sides of Eq. 2 by u_{rs}^{α} for the first equation and p_{rs}^{α} for the second equation, and integrating over Γ, the orthogonality of the condensation functions alongside Eq. 3 gives:

$$\begin{cases} u_{rs}^1 = u_{rs}^2 \\ p_{rs}^1 = -p_{rs}^2 \end{cases}. \tag{4}$$

Substituting Eq. 1 into Eq. 4 and assembling all equations into a matrix form give:

$$-[\mathbf{Z}_\mathbf{C}^1 + \mathbf{Z}_\mathbf{C}^2]\mathbf{U_c} = \mathbf{P_e}, \tag{5}$$

where $\mathbf{Z_C}$ is the matrix of the condensed impedance of an acoustic sub-system over the interface; $\mathbf{U_c}$ and $\mathbf{P_e}$ are the velocity and the blocked pressure induced by the sound source. Detailed derivation procedure can be found in [3]. The coupled velocity on Γ can be finally resolved as

$$\mathbf{U_c} = -[\mathbf{Z}_\mathbf{C}^1 + \mathbf{Z}_\mathbf{C}^2]^{-1}\mathbf{P_e}. \tag{6}$$

2.1.2 The Piecewise calculation scheme

To warrant the convergence of the method, N_x and N_y should be selected in such a way that a sufficient number of CF functions are used per wavelength to cover the maximum frequency of interest. However, for the mid-to-high frequency modelling, the computational time would significantly increase as the matrix size becomes larger. It was shown recently that the convergence rule can be further relaxed if the CFs can match the oscillating wave feature over the coupling interface, exemplified by the complex exponential:

$$\varphi_{rs}(x,y) = \frac{1}{\sqrt{L_x L_y}} \exp\left(i\frac{2r\pi x}{L_x}\right)\exp\left(i\frac{2s\pi y}{L_y}\right), \tag{7}$$

in which $r \in [0, \pm1, \pm2, \ldots, \pm N_x]$, $s \in [0, \pm1, \pm2, \ldots, \pm N_y]$. The function wavelength of each $\varphi_{rs}(x,y)$ is defined as:

$$\lambda_{c,rs}(x,y) = \frac{2\pi}{\sqrt{\left(\frac{2r\pi}{L_x}\right)^2+\left(\frac{2s\pi}{L_y}\right)^2}}. \tag{8}$$

For a targeted frequency band $[f_l, f_h]$, corresponding to a wavelength range $[\lambda_h, \lambda_l]$, it has been shown that, for a plate-cavity system, the condensed velocity $\mathbf{U}_c$ would converge by only including those dominating terms φ_{rs} which satisfy $\lambda_h < \lambda_{c,rs} < \beta\lambda_l$, with β =1.5 [3]. The truncated series is also shown to dominate the condensed impedance matrix and the condensed mobility matrix. As a result, the piecewise scheme can reduce the size of the matrix to be inversed on the right-hand side of Eq. 6 so that the computational time can be significantly shortened. In this paper, we will investigate the validity of this criterion in the cases of coupled cavities with different coupling strength. Theoretically, the scheme can be applied to pure structural coupling cases. Instead, CTF had already be validated and applied to different mechanical structures

([14]). One can expect that the piecewise sscheme remains valids for the coupling of homogeneous structures (for instance, for coupled panels with constant thicknesses). For heterogeneous structures exhibiting different types of waves that can be coupled together, the criterion related to the piecewise scheme should certainly adapted. More investigations that are outside the scope of the present paper should be carried out in the future.

2.2 Coupling strength

2.2.1 Quantification of the coupling strength

Based on the physical implication of the coupling, as described in Introduction, the coupling strength is quantified by evaluating the acoustic pressure differences over the coupling interface before and after the attached sub-cavity is added: *e.g.* $|\boldsymbol{P}_C - \boldsymbol{P}_e|$ where $\boldsymbol{P}_\mathrm{C}$ and $\boldsymbol{P}_\mathrm{e}$ are the acoustic pressure over the interface before and after the coupling. In light of Eq. 6, one has

$$\mathbf{P_c} = -\mathbf{Z}_\mathbf{C}^2[\mathbf{Z}_\mathbf{C}^1 + \mathbf{Z}_\mathbf{C}^2]^{-1}\mathbf{P_e}. \tag{9}$$

When $\mathbf{P}_\mathrm{C} \approx \mathbf{P}_e$, the coupling is considered to be weak.

To quantify the coupling strength, a coupling strength factor Ω is defined, also to be further used to assist the validations of the piecewise scheme under different coupling strength conditions. Define the coupling strength matrix $\mathbf{S} = -\mathbf{Z}_\mathrm{C}^2[\mathbf{Z}_\mathrm{C}^1 + \mathbf{Z}_\mathrm{C}^2]^{-1}$ from Eq. 9. ~~Because $\mathbf{Z}_\mathbf{C}^1$ and $\mathbf{Z}_\mathbf{C}^2$ are both invertible,~~ (RK: I do not see the link between the fact that Z are both invertible and the diagonalization of S…As Z and the inverse of Z are symmetric (if we neglect the damping effect), S is symmetric and then, diagonalizable… I think it is better to say nothing…). From an eigendecomposition, $\mathbf{S}$ can be rewritten as $\mathbf{S} = \mathbf{K}^{-1}\boldsymbol{\Lambda}\mathbf{K}$ where the columns of $\mathbf{K}$ are the eigenvectors of $\mathbf{S}$

and $\mathbf{\Lambda}$ is a diagonal matrix containing the corresponding eigenvalues of $\mathbf{S}$. For a acoustic sub-system weakly coupled with another one (i.e. $\mathbf{P}_C \approx \mathbf{P}_e$), all the eigenvalues are then close to one. In contrary, for strongly coupled acoustic subsystems (i.e. $\mathbf{P}_C \neq \mathbf{P}_e$), the eigenvalues are different than one~~. λ_N is positively correlated with the response level p_N of the Nth condensation function and the response level is smaller when an attached sub-system is added~~. Thus, we define the coupling strength parameter

$$\Omega = \left|1 - \frac{\sum_N \lambda_N}{N}\right| \tag{10}$$

where N is the dimension of $\mathbf{S}$ (i.e. $N = N_x N_y$) and λ_N is the Nth eigenvalue of $\mathbf{S}$. The summation of the eigenvalues can be replaced by the trace of $\mathbf{S}$ that avoid the explicit calculation of the eigenvalues. Ω should increase as the coupling strength becomes stronger. For instance, Ω equals to zero when there is no coupling and equals to one when the attached sub-system is equivalent to a pressure release boundary. Additionally, Ω is independent of the type and number of the selected condensation functions, so long as the convergence rules are satisfied.

2.2.2 Numerical validations and discussions on the coupling strength factor

In this section, the relationship between the proposed Ω and the acoustic response differences over the coupling interface before and after coupling will be validated using an acoustic cavity shown in Fig. 2. The system contains two sub-cavities connected through an opening, which is commonly used in vibro-acoustic analyses [22, 23]. The main sub-cavity has a fixed dimension (x×y×z) 2.5×2×1.5 (m).

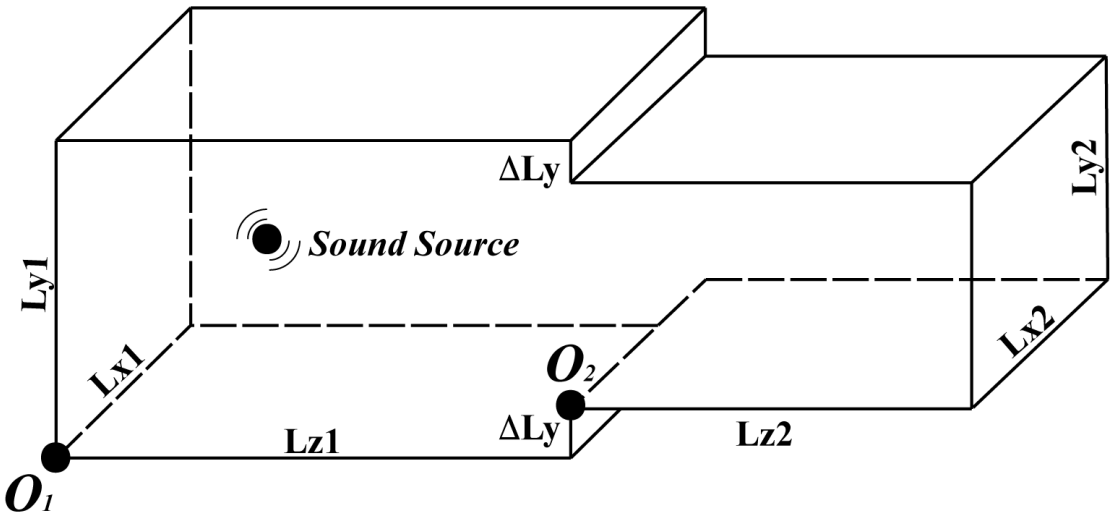

Figure 2 Configurations of the coupled acoustic system, excited by an internal sound source in the main sub-cavity.

The uncoupled acoustic pressure p within the cavity satisfies the wave equation and the associated boundary condition:

$$\nabla^2 p(r,t) - \frac{1}{c_0^2}\frac{\partial^2 p}{\partial t^2}(r,t) = -\rho_0 \dot{Q}(t)\delta(r-r_0), \tag{11}$$

$$\frac{\partial p}{\partial n} = 0 \qquad \text{on the boundary,} \tag{12}$$

where r_0 is the location of the sound source, Q is the volume velocity strength of the sound source, ρ_0 and c_0 are the equilibrium air density and the acoustic velocity within the cavity, respectively. Because the two cavities can be modelled following the same procedure, the superscript α representing the sub-system number is omitted for convenience. In the harmonic regime, one can solve ~~$p(r)$ from~~ Eqs. 11 and 12 using a modal expansion:

$$p(r) = \frac{i\omega\rho_0 c_0^2 Q}{V}\sum_m \frac{\phi_m(r)\phi_m(r_0)}{\Lambda_m(\omega_m^2 - \omega^2 + 2i\xi\omega_m\omega)}, \tag{13}$$

where ϕ_m is the mth acoustic mode of the rigid-walled cavity; ω_m is the mth natural frequency; ξ is the damping ratio and assumed to be equal for all cavity modes; V is the

volume of the cavity, and $\Lambda_n = \int \phi_n^2 dV/V$. An analytical expression of the acoustic modes of the rectangular cavities will be considered in the following. One can underline that for the practical cases with cavities of complex geometry, FEM can be used to obtained the modal information as well. Substituting Eq. 13 into Eq. 2, one obtains the free condensed pressure $\tilde{p}_{rs}$ as:

$$\tilde{p}_{rs} = \frac{i\omega\rho_0 c_0^2 Q}{V} \sum_m \frac{\phi_m(r_0) C_{rs,m}}{\Lambda_m(\omega_m^2 - \omega^2 + 2i\xi\omega_m\omega)}, \tag{14}$$

where $C_{rs,m} = \int \varphi_{rs}\phi_m dS$ is the modal matching coefficient between the *r*sth CF and the *m*th acoustic mode. By the same way, using Eq. 1, the condensed impedance $z_{kl,rs}$, is given by:

$$z_{kl,rs} = \frac{i\omega\rho_0 c_0^2}{V} \sum_m \frac{C_{kl,m} C_{rs,m}^*}{\Lambda_m(\omega_m^2 - \omega^2 + 2i\xi\omega_m\omega)}. \tag{15}$$

~~By substituting~~ Eqs. 14 and 15 give us respectively, the ~~free~~ blocked condensed pressure vector $\mathbf{P_e}$ and the condensed impedance matrix $\mathbf{Z}_\mathrm{C}^1$ and $\mathbf{Z}_\mathrm{C}^2$. These quantities can be introduced in into Eq. 6. The velocity over the interface between the two sub-cavities can then be solved either in a full or piecewise manner.

In order to highlight the parameters influencing the coupling strength matrix **S,** one can rewrite it as

$$\mathbf{S} = [\mathbf{I} + \mathbf{Z}_\mathrm{C}^1 (\mathbf{Z}_\mathrm{C}^2)^{-1}]^{-1}. \tag{16}$$

in which $\mathbf{Z}_\mathrm{C}^1 (\mathbf{Z}_\mathrm{C}^2)^{-1}$ can be further expanded as:

$$\mathbf{Z}_\mathrm{C}^1 (\mathbf{Z}_\mathrm{C}^2)^{-1} = \frac{V_2}{V_1} \begin{bmatrix} \vdots & \cdots & \vdots \\ \cdots & \ddots & \cdots \\ \vdots & \cdots & \sum_m \frac{C_{kl,m} C_{rs,m}^*}{\Lambda_m(\omega_m^2 - \omega^2 + 2i\xi\omega_m\omega)} \end{bmatrix} \begin{bmatrix} \vdots & \cdots & \vdots \\ \cdots & \ddots & \cdots \\ \vdots & \cdots & \sum_n \frac{C_{kl,n} C_{rs,n}^*}{\Lambda_n(\omega_n^2 - \omega^2 + 2i\xi\omega_n\omega)} \end{bmatrix}^{-1}, \tag{17}$$

where m is the modal order of the main sub-cavity and n is the modal order of the attached sub-cavity. It can be seen from Eq. 17 that there are three factors that influence the coupling strength: volume ratio of the two sub-cavities, frequency dependent terms, and the spatial modal matching terms. For the volume ratio, the weak coupling occurs when $V_2/V_1 \ll 1$. For a given main sub-cavity volume V_1, the coupling strength increases with V_2. One should notice that the volume ratio is only valid for the current double-sub-cavity configuration. The second factor is the modal matching term $C_{kl,m}C^*_{rs,m}$, which is non-dimensional and determined by the spatial matching level between the CFs and the mode shapes of the two sub-systems. As for the frequency-dependent part, one would intuitively guess the strong coupling happens at resonances. Particularly when the two cavities share the same resonance frequency in low frequency range, the coupling process can be referred to the working mechanism of an acoustic resonator within an enclosure. However, in the mid-to-high frequency range, it is less relevant to focus on a single frequency but more reasonable to average it within a frequency band as $\frac{1}{\Delta f}\int_f \Omega df$.

For the present cavity configuration, the coupling strength is quantified based on the pressure differences over the interface with and without the attached sub-cavity, defined as:

$$D = \frac{1}{S}\int_S \frac{|P_e - P_C|}{|P_e|} dS. \tag{18}$$

D can be averaged in a frequency band as $\frac{1}{\Delta f}\int_f Ddf$ as well. To eliminate the influence of the sound source location, P_e is not obtained by setting a particular sound source but assumed to be unit on all basis functions as

$$P_e = \begin{bmatrix} \varphi_{11} \\ \cdots \\ \varphi_{rs} \end{bmatrix}. \quad (19)$$

With such definition, Ω should reflect the variation trend of *D* when the dimension/volume of the attached sub-cavity changes, as shown in Fig. 3, as a function of volume ratio by setting ΔLy=0 and varying Lz2. Both *D* and Ω are averaged in two selected frequency bands with a 200Hz bandwidth, centered at 1100 Hz and 1500 Hz, respectively. Ω obtained from the truncated series using piecewise scheme criterion is also shown for reference. It can be seen that Ω is only slightly affected by the truncated series so long as the solution converges. Therefore, Ω will be calculated using the truncated series in the piecewise scheme in the following analyses. It can be observed in Fig. 3 that *D* and Ω undergo the same variation trend as a function of V_2/V_1 and both, albeit not monotonously, exhibit an overall increasing trend with V_2/V_1. Fluctuations can be attributed to the resonances of the coupled system. Both *D* and Ω reach a local maximum value of 0.5 when V_2/V_1=1. It can be surmised that *D* and Ω will not be larger than 0.5 until $V_2 \gg V_1$, where V_2 can be approximately considered as infinitely larger than V_1. Since we only aim at modelling the coupling process between two sub-systems with comparable sizes, the case of $V_2 \leq V_1$ will be the main focus of analyses in this paper. To better show the consistent variation trend between *D* and Ω, *D* is plotted as a function of Ω in Figs. 4a and 4b, averaged in the same two frequency bands. It can be seen that Ω is approximately proportional to *D*, i.e. the proposed coupling strength factor could effectively reflect the response differences over the interface as well as the coupling strength, in agreement with our intuitive understanding.

It should be noticed that all the above analyses can be repeated in a vibro-acoustic system as well. Similar theoretical model and numerical validation for a plate-cavity system are presented in Appendix.

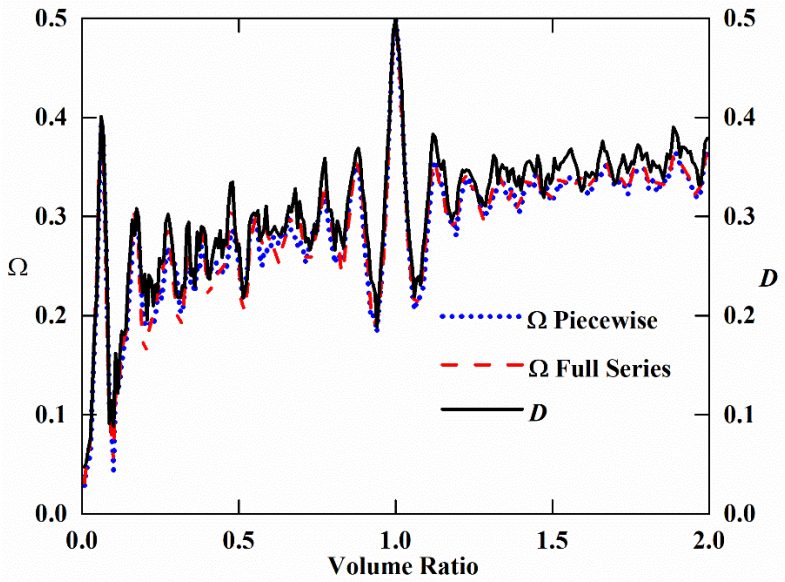

(a)

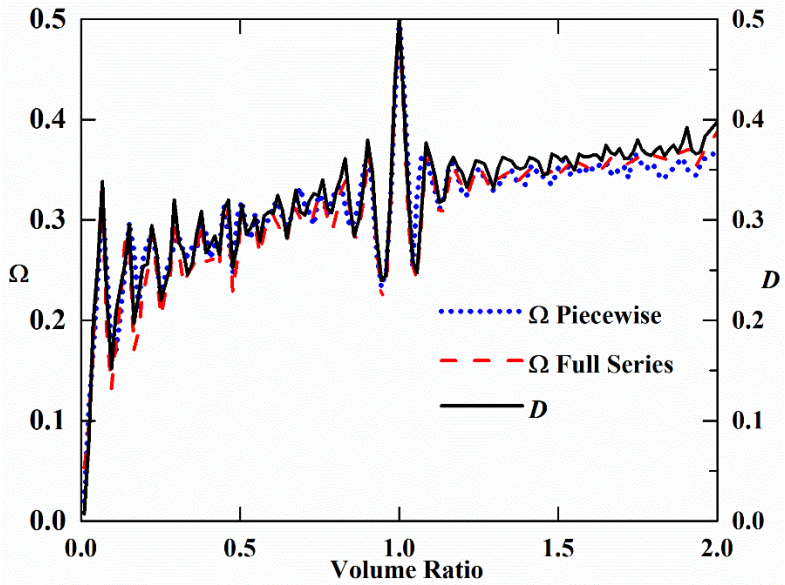

(b)

Figure 3 Interface pressure response differences *D* and the coupling strength factor Ω as functions of the volume ratio, averaged in frequency bands of 200Hz wide centered at: (a) 1100 Hz; (b) 1500 Hz.

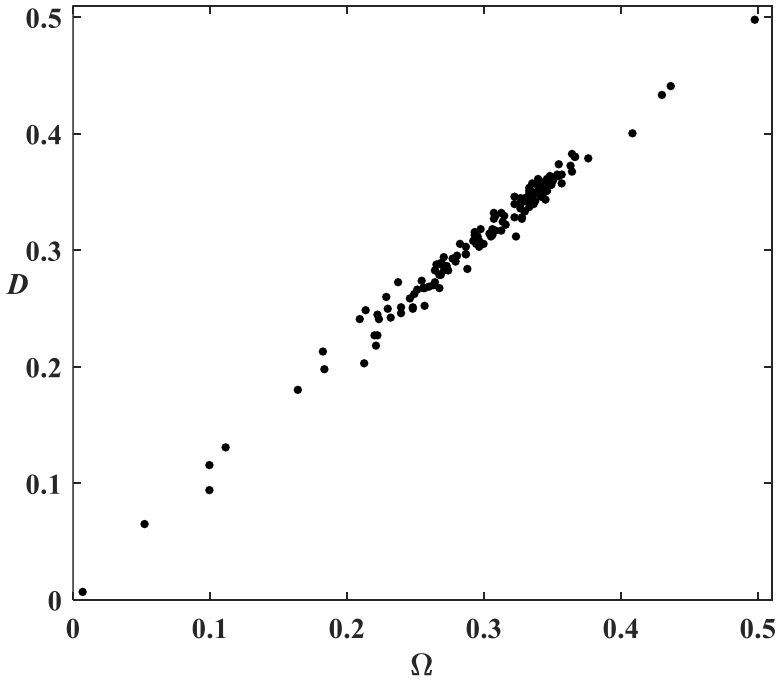

(a)

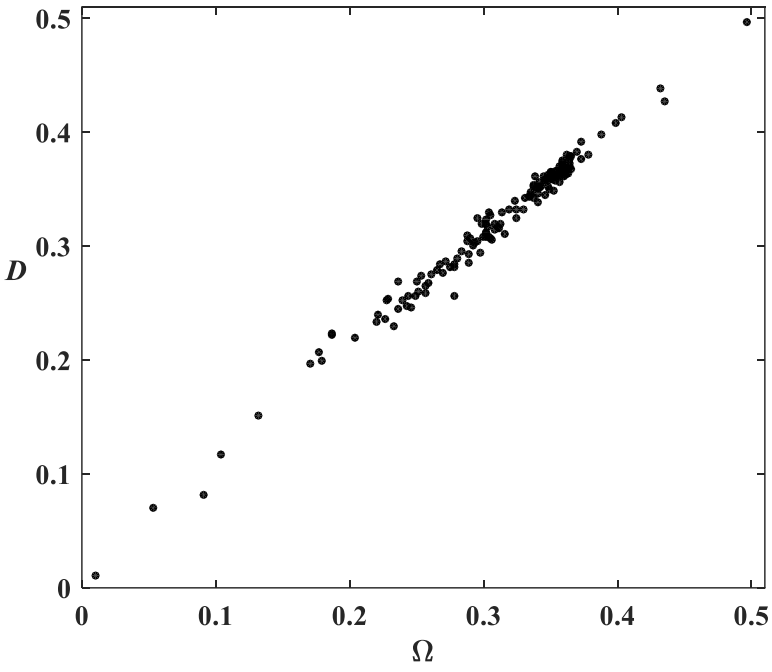

(b)

Figure 4 Relationship between the interface pressure response differences *D* and the coupling strength factor Ω, averaged in frequency bands of 200Hz wide centered at: (a) 1100 Hz; (b) 1500 Hz.

3. Numerical Analyses

All numerical analyses are implemented based on the configuration shown in Fig. 2. Before going into error analyses, some validations are presented by comparing the piecewise calculation results and the analytical solutions obtained by setting ΔLy=0 and Lz2=Lz1. Notice that this configuration has the strongest coupling strength (Ω=0.5) among the considered cases. Then, the computational error of the piecewise scheme will be examined under different coupling strength levels.

3.1 Validation of the piecewise scheme in the strong coupling case

By setting ΔLy=0, the main sub-cavity and the attached sub-cavity form a rigid rectangular cavity so that the analytical solution can be obtained as the reference result. The CTF-based piecewise calculation scheme treats the cavity as two sub-systems. β is selected to be 1.5 in this paper, because the tendency of error convergence is found to be similar to that in the previous work [3]. Comparisons in terms of the sound pressure level (SPL) are made at two arbitrarily receiving points, located in the sub-cavities 1 and 2 respectively. The results are shown in Fig. 5, in which only the results in mid-to-high frequency bands are presented. The dotted line, obtained from the piecewise scheme, includes 4 individual piecewise calculations, each with a 200 Hz bandwidth. Note a broader band will reduce the computational efficiency and dilute the advantage of the method. Nevertheless, a broader computational band could increase the accuracy of the method due to the inclusion of more CF terms, because the equivalent β for entire frequency band becomes larger. The results obtained from the

full CTF calculation are also shown as reference. It can be observed that the piecewise calculation can well capture the SPL especially for those resonance peaks. Although errors exist at some anti-resonance frequencies, they are not the major concern of the mid-to-high frequency problem. Figure 6a shows the sound pressure distribution, obtained from the piecewise scheme, over the coupling interface at 1100 Hz. The result is consistent with that obtained from the analytical solution in Fig. 6b. Similar accuracy was also found to exist at other receiving points and cut surfaces (not shown here). Figure 7 shows the volume-averaged SPL within each 200 Hz bandwidth. It can be observed that the errors are capped at around 2 dB. Notice these errors can be reduced by enlarging the computational bands. The errors are found to be less than 1 dB when the same calculations are conducted within the one third octave bands centered at 1250 Hz and 1600 Hz.

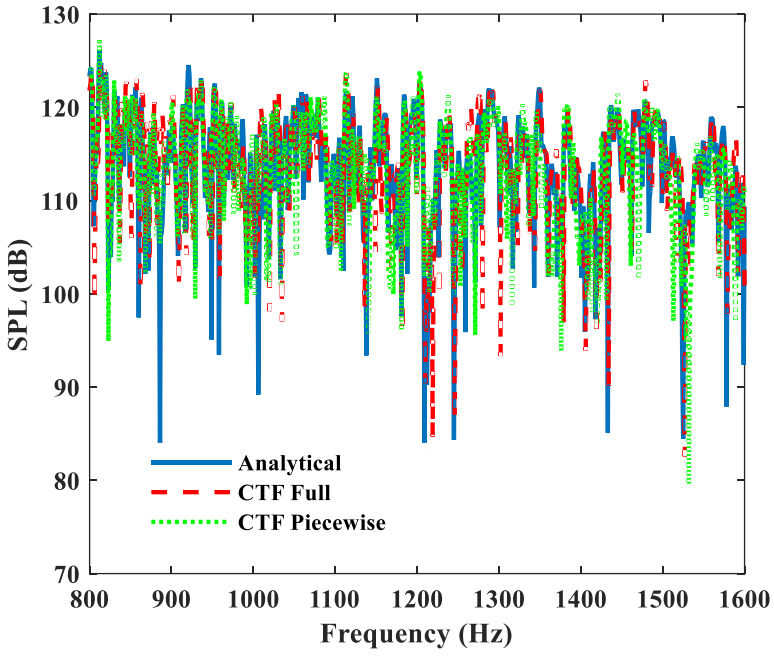

(a)

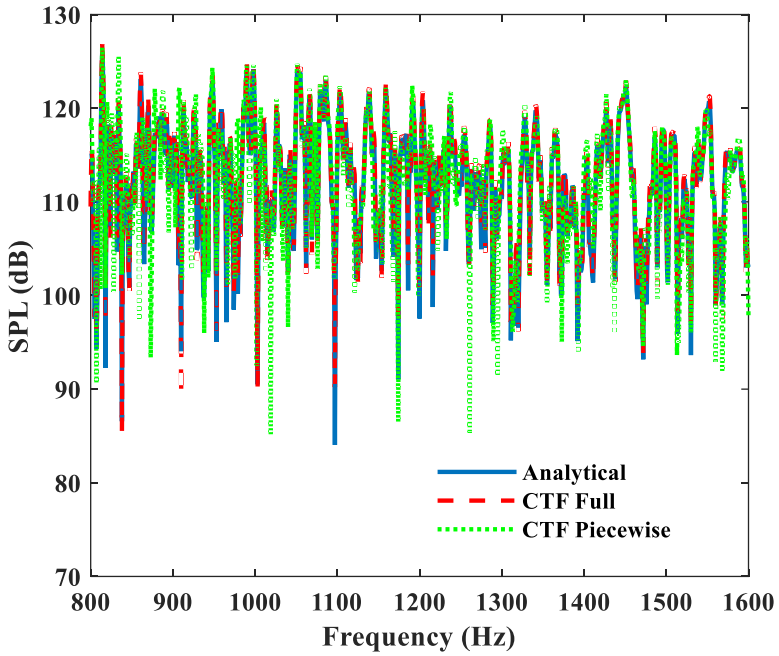

(b)

Figure 5 SPL at: (a) (1.7, 1.3, 1.2) m in the main cavity; (b) (2.1, 0.6, 0.9) m in the attached cavity.

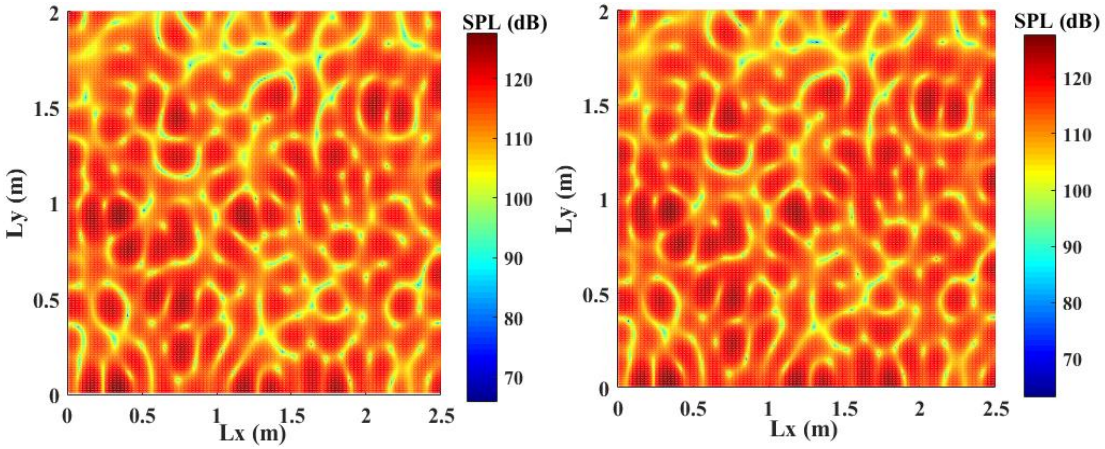

(a) (b)

Figure 6 SPL distribution over the coupling interface: (a) Piecewise scheme; (b) Analytical solution.

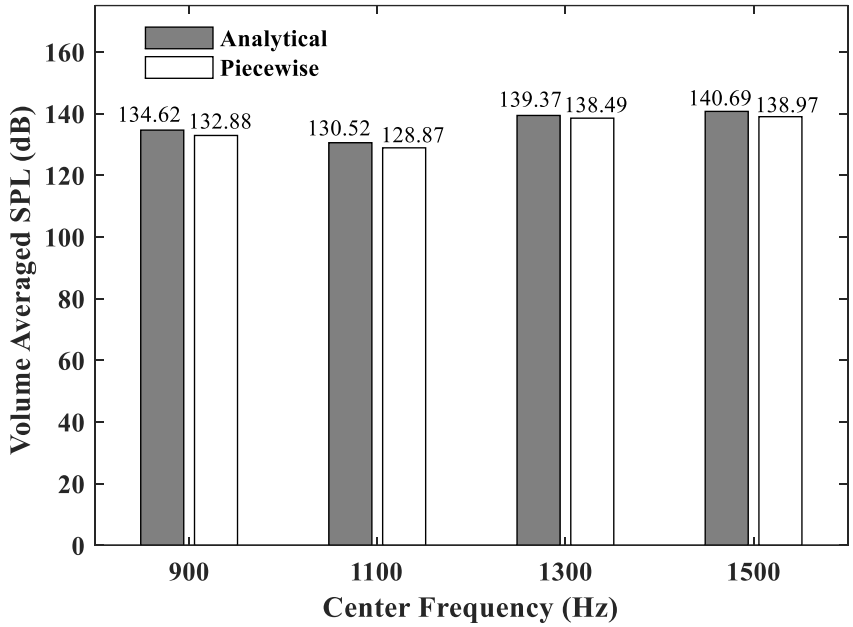

Figure 7 Volume-averaged SPL within frequency bands of 200 Hz wide: analytical solution and piecewise scheme.

The above results numerically validate the piecewise scheme in a strongly coupled system. The method well balances the efficiency and accuracy within mid-to-high frequency ranges. In addition, it can provide a detailed prediction of the acoustic field in both sub- systems, which is the most appealing advantage over the SEA.

3.2 Error analyses of the piecewise scheme with variable coupling strength

In this section, the influence of the coupling strength on the accuracy of the piecewise calculation scheme will be investigated. As discussed in Section 2.2.2, the coupling strength is mainly determined by the volume ratio and the modal matching matrix in the mid-to-high frequency range. Therefore, firstly these two factors are separately investigated and then a general conclusion is drawn at the end of this section to conclude the relationship between the coupling strength and the performance of the piecewise scheme. For analyses purposes, the error of the piecewise calculation scheme is defined within a given frequency band Δf as:

$$E_c = \frac{1}{S\Delta f}\int_{\Delta f}\int_S \left|P_{pw} - P_c\right| dSdf, \tag{20}$$

where P_{pw} is the piecewise solution and P_c the full CTF calculation or analytical solution whenever available.

3.2.1 Effect of the volume ratio

This subsection discusses the effect of the volume ratio on the performance of the piecewise calculation scheme~~, by using the same configurations as those used in Fig. 3~~. The volume ratio is adjusted by enlarging L_{z2} from 0.15m to 1.5m. As a reference, the coupling strength factors of the analyzed configurations are shown in Fig. 8a. As stated, only $V_2 < V_1$ is considered here. Figures 8b shows the errors of the piecewise scheme for two frequency bands of 200 Hz wide, centered at 1100 Hz and 1500 Hz, respectively. It can be observed in Fig. 8b that E_c becomes larger as the volume ratio V_2/V_1 increases. Comparisons between Figs. 8a and 8b show that E_c increases as the coupling strength gets stronger. The maximum value of E_c is between 1.6 to 1.8 dB when $V_2 = V_1$, which is still within the general tolerance level for the mid-to-high frequency modeling. For the detailed performance analysis at the maximum error, one can refer to Section 3.1.

It is worth noticing that the relatively large E_c only arises when the volume ratio V_2/V_1 is close to one, when the two cavities are identical. In this case, neither cavity is more deterministic nor statistical than the other. This shows the capability of the piecewise calculation scheme in solving strongly coupled systems where deterministic-statistical methods are no longer applicable to provide detailed system responses of the whole system.

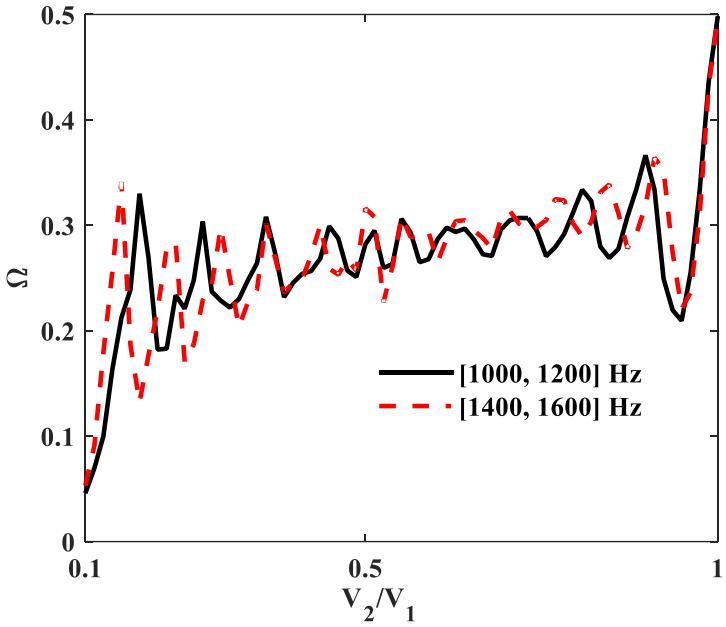

(a)

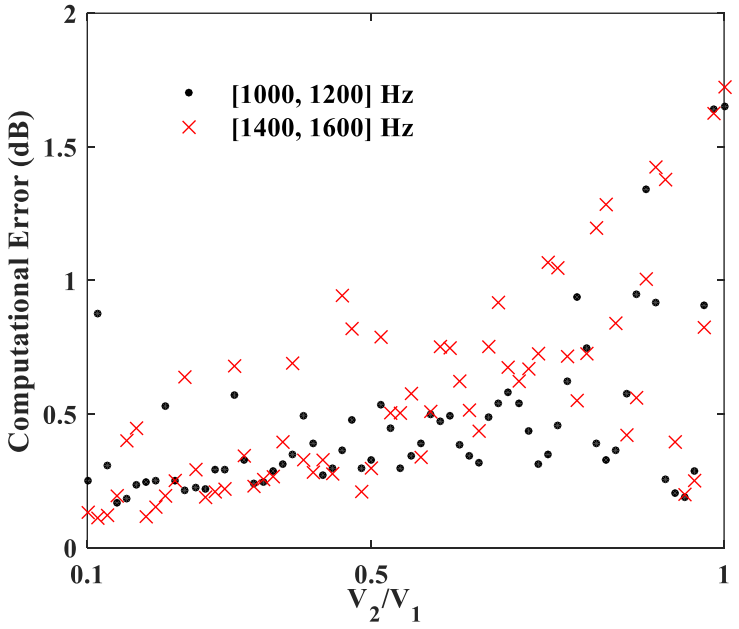

(b)

Figure 8 Surface velocity error of the piecewise scheme with respect to different volume ratios in frequency bands of 200 Hz wide centered at: (a) 1100 Hz; (b) 1500 Hz.

3.2.2 Effect of the interface modal matching

The effect of the interface modal matching on the performance of the piecewise scheme is investigated in this subsection. Different from the volume ratio, appearing as an amplification coefficient in Eq. 17, the modal matching matrix is directly determined by the piecewise scheme. The variation of the interface modal matching is achieved by increasing ΔLy from 0 to 0.5m, as shown in Fig. 2. When ΔLy=0.5m, the interface area becomes half of its largest value. To keep the volume ratio constant at one, the depth of the attached cavity Lz2 is automatically adjusted. All analyzed quantities are frequency averaged within the two frequency bands which are the same as in Fig. 8.

Firstly, the coupling strength factors are plotted for different ΔLy in Fig. 9a. It can be observed that the coupling strength generally decreases as ΔLy gets larger, corresponding to a smaller interface area, in line with one's intuition. However, this is not simply due to the smaller interface area because $C_{kl,m}C^*_{rs,m}$ is not only determined by the area but also depends on the wave matching level over the interface, which is very complex in the mid-to-high frequency range. For the present case, the variation trend of Ω indicates that the modal matching level becomes smaller as ΔLy decreases, since the influcnes of the volume ratio and frequency are excluded in the simulations.

The computational errors for different ΔLy are shown in Fig. 9. Again, one observes the similar variation trends as the coupling strengths have. As ΔLy increases, the computational errors quickly drop at the beginning and converge to a small value around 0.2 dB. The same conclusion as in Section 3.2.1 can be drawn in that the computational error is larger when the two cavities are similar. This verifies the capability of the piecewise scheme in strong coupled cases where the modal matching levels are different.

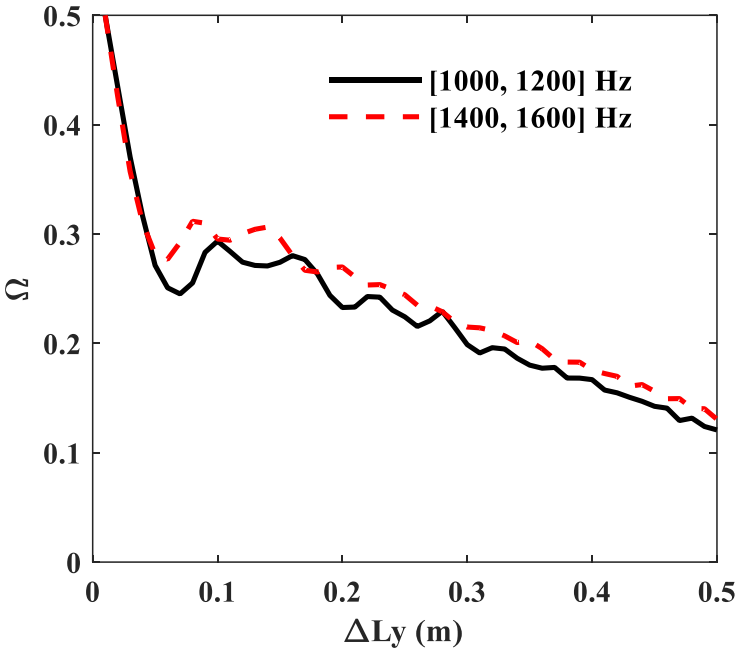

(a)

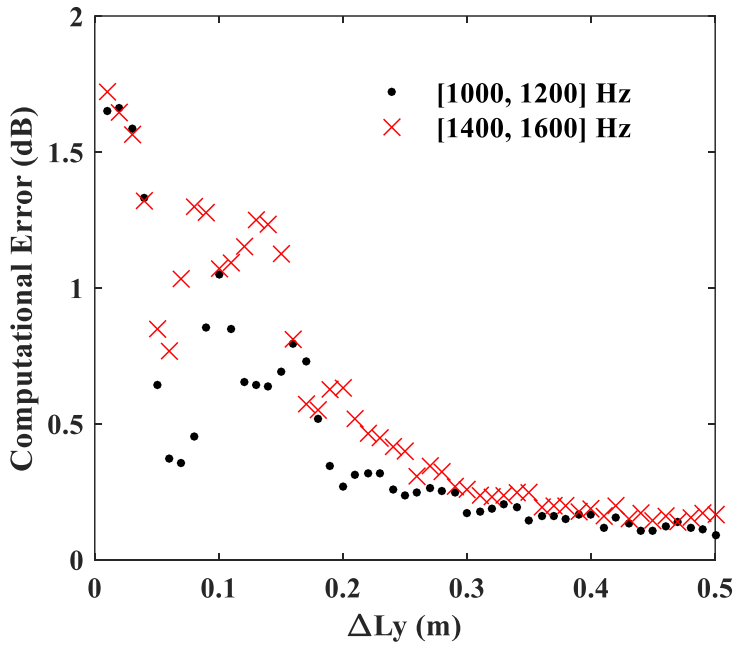

(b)

Figure 9 Surface velocity error of the piecewise scheme with respect to different modal matching in frequency bands of 200 Hz wide centered at: (a) 1100 Hz; (b) 1500 Hz.

3.2.3 Effect of the coupling strength as quantified by Ω

To summarize the above analyses results, the computational data used in Figs. 3, 8 and 9 are rearranged and regrouped to plot the computational error E_c as a function of the coupling strength Ω, obtained from different volume ratios and modal matching matrix and averaged in [1000, 1200] Hz and [1400, 1600] Hz, respectively. These results in a total of four sets are shown in Fig. 10 with different types of marker. It can be observed that, irrespective of the way in which the coupling strength is obtained, the errors at any given Ω are rather consistent in trend and close in values. For relatively weak coupling strength, when Ω is smaller than 0.2, the error of the piecewise scheme is rather stable and dwells around 0.2 dB. When Ω becomes larger than 0.2, the error undergoes fast increases before gradually stabilizing when Ω is larger than 0.4. It should be noted that, between 0.2 and 0.4, the increasing speed of the error is not exactly the same because the piecewise scheme has different sensitivities to volume ratio, modal matching level and frequency bands. It is also relevant to note that a higher frequency band exhibits a larger error. One of the plausible reasons is the wave motion over the interface is more complex in a higher frequency band so that a wider calculation bandwidth Δf compared to its center frequency would be needed to warrant an more accurate prediction. However, this can be avoided by considering the one-third octave or octave bands as people usually do in mid-to-high frequency modelling problems.

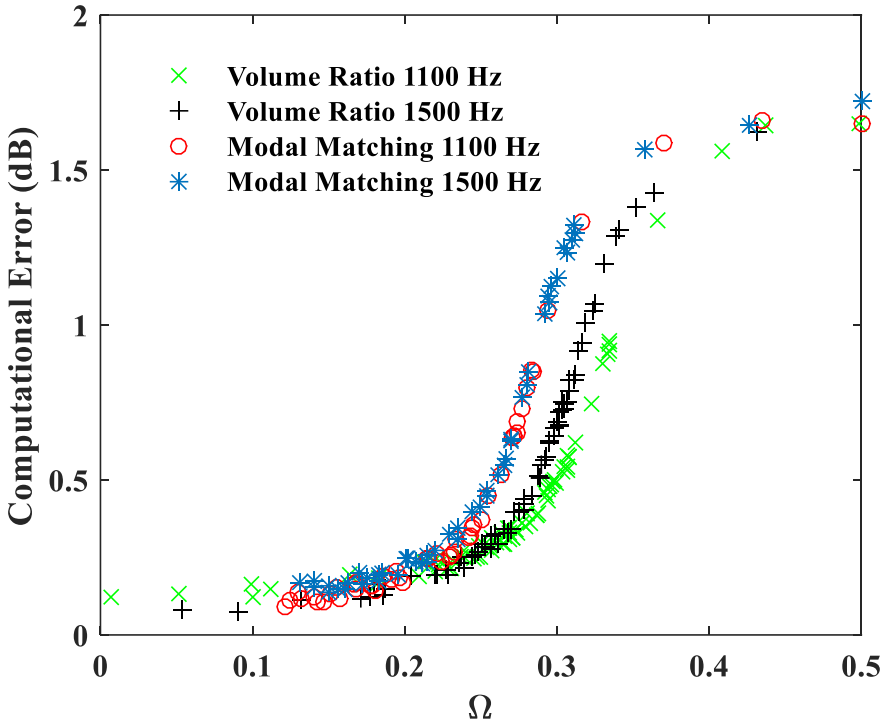

Figure 10 Computational error E as a function of the coupling strength varied with volume ratio or modal matching matrix, averaged within [1000, 1200] Hz and [1400, 1600] Hz.

4. Experimental validations

Experimental validations were carried out using the configuration shown in Figs. 11a and 11b. The cavity walls were made of acrylic of 30mm thickness which can be considered as acoustically rigid. A loudspeaker was used to generate an acoustic excitation through a hole drilled at (0.075, 0.05, 0) m over the side wall. Microphones 1 and 2 were installed at (0.075, 0.05, 0.01) mm and (0.25, 0.15, 0.83) m, respectively, to measure the transfer function between them and eliminate the sound source error at the same time [24]. Limited by the experimental conditions, the cavity dimensions are smaller than those used in the previous simulations. However, a higher frequency band up to 3200 Hz was selected instead. For reference, the volume ratio V_2/V_1 is 0.94.

The experiment was conducted within a wide frequency band of [40, 3200] Hz, with results shown in Figs. 12a and 12b, respectively. It was shown in the previous work [3] that the piecewise scheme starts to be applicable when the modal overlap factor is larger than one. In the present test structure, the unit modal overlap factor is approximately at 1200 Hz. Therefore, the full CTF calculation is used within [40, 1200] Hz and the piecewise scheme is used within [1200, 3200]. To obtain more accurate peak values at resonance frequencies, the damping ratio of the first four peaks are obtained from the experimental result while the others are all set to 0.001. It can be observed in Fig. 12a that the full CTF calculation result agrees well with the experimental one, in terms of both resonance and anti-resonance frequencies as well as the overall trend. The piecewise calculation (Fig. 12b) was conducted within ten frequency bands of 200Hz bandwidth and added up to [1200, 3200] Hz. It can be seen that the piecewise scheme can accurately capture the variation trend and most of the resonance peaks. The few missing peaks in the experimental curve can be attributed to the machining tolerance of the cavity and some unavoidable uncertainties. All in all, the validity of the piecewise calculation scheme is considered to be verified in such a highly dynamic and strongly coupled system.

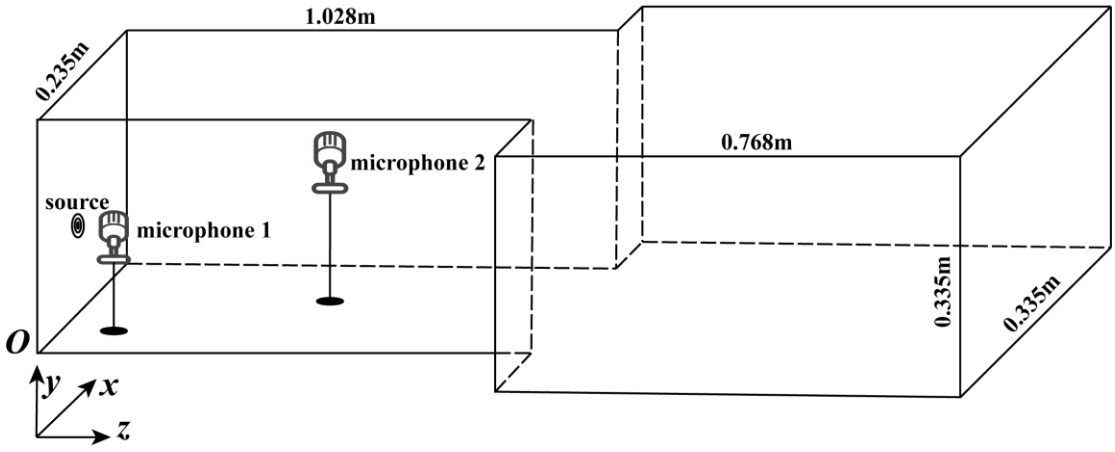

(a)

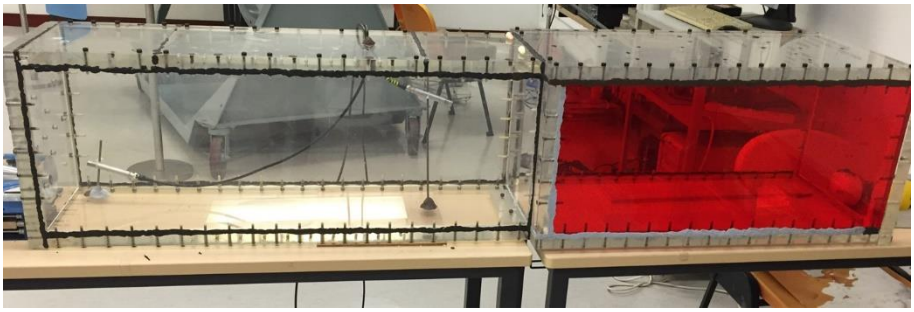

(b)

Figure 11 The cavity where the experiments conducted: (a) Cavity configuration; (b) Photo of the cavity.

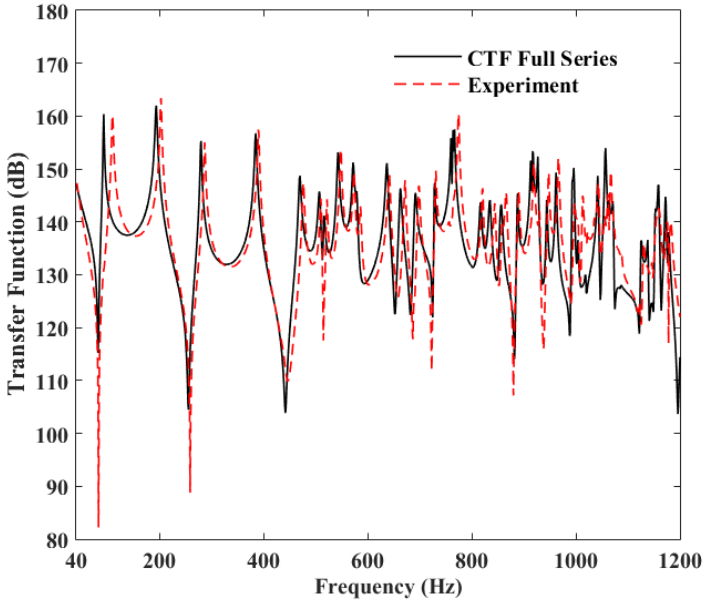

(a)

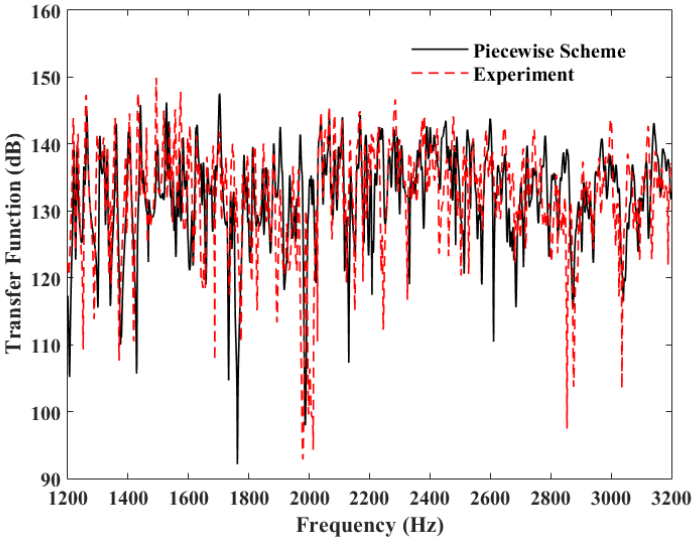

(b)

Figure 12 Predicted transfer function between two points, compared to the experimental result: (a) Full CTF calculation; (b) Piecewise scheme.

5. Conclusions

This paper extends the application range of a previously proposed piecewise calculation scheme to strong coupling cases. The coupling strength is defined by examining the acoustic response differences over the coupling interface before and after the attached sub-system is added. A coupling strength factor Ω is established to quantify the coupling strength in the context of multi-degree-of-freedom system and mid-to-high frequency range. With the assistance of Ω, the computational errors of the piecewise scheme are investigated through tactically adjusting the coupling strength level, including the strongly coupled systems. Generally, the proposed piecewise calculation scheme is shown to be applicable in strongly coupled cases, by showing a good agreement with the analytical solutions and the experiment results. Main conclusions are summarized as follows.

1. The proposed coupling strength factor Ω can well reflect the variation trend of the coupling strength between two coupled sub-systems, as reflected by the acoustic response differences over the coupling interface. Three factors are found to affect the coupling strength between two acoustic sub-cavities: volume ratio, interface modal matching level and the frequency. Similar quantification can also be achieved for structural-acoustic coupled system as detailed in Appendix. By comparing the value of Ω, the coupling strength in an acoustically coupled system is shown to be generally much stronger than that of the structure-cavity system.

2. The piecewise calculation scheme is shown to be effective and accurate enough in the modelling of a strongly coupled acoustic cavity. Without losing the efficiency and compromising its accuracy, the proposed scheme allows a detailed sound field description of each sub-system.

3. The computational error increases when the coupling strength becomes stronger, which, nevertheless, is still within the normal tolerance level in terms of the mid-to-high frequency modelling. For a given system and a prescribed frequency band, the computational error of the piecewise calculation scheme can be approximately evaluated from Ω..

Appendix

A similar analysis is conducted for a structure-acoustic coupled system, exemplified by a plate-cavity system. Referring to Fig. 1, the main sub-system is set to be a plate while the attached sub-system is still an acoustic cavity and only structural excitation exists.

For a structural sub-system, the mobility is preferred instead of the impedense to avoid the singularity problem. In such cases, the condensed mobility $Y_{kl,rs}$ can be similarly defined by imposing a prescribed pressure $P(x,y) = \varphi_r(x)\varphi_s(y)$ on Γ as:

$$Y_{kl,rs} = \frac{<\bar{U}_{rs},\varphi_{kl}>}{<P,\varphi_{rs}>} =< \bar{U}_{rs}, \varphi_{kl} >, \tag{A1}$$

where $\bar{U}_{rs}$ is the uncoupled free velocity on Γ when the subsystem is subjected to $P(x,y)$. Then, the condensed mobility of the plate writes:

$$Y^s_{pq,kl} = \frac{i\omega}{\rho_s h}\sum_m \frac{C_{pq,m}C^*_{kl,m}}{\Lambda_m(\omega_m^2-\omega^2+2i\xi^s\omega_m\omega)}, \tag{A2}$$

where ρ_s is the density of the plate; h the plate thickness; ξ^s the damping ratio of the plate assumed to be equal for all the modes; ω_m the natural frequency of the mth plate mode. $\Lambda_m = \int \phi_m^2 dV$ and $C_{pq,m} = \int \varphi_{pq}\phi_m dS$ where ϕ_m is the mth mode shape. Similar to Eq. 6, the velocity over the interface can be expressed as

$$\mathbf{U_c} = -[(\mathbf{Y_C^1})^{-1} + \mathbf{Z_C^2}]^{-1}\mathbf{P_e}, \tag{A3}$$

where $\mathbf{P_e}$ is the external excitation in CF coordinate rather than the blocked pressure as in Section 2. The weak coupling strength can be identified by rearranging Eq. A3 into

$$\mathbf{U_c} = -[(\mathbf{Y_C^1})^{-1} + \mathbf{Z_C^2}]^{-1}(\mathbf{Y_C^1})^{-1}\mathbf{U}_f \approx \mathbf{U}_f \tag{A4}$$

where $\mathbf{U}_f$ is the free velocity of the structure when structurally excited. The coupling strength can be quantified as in Eq. 9:

$$\mathbf{S} = -[\mathbf{I} + (\mathbf{Y_C^1})(\mathbf{Z_C^2})]^{-1}, \tag{A5}$$

Then Ω can be obtained from the matrix trace of $\mathbf{S}$. The difference between Eq. A5 and Eq. 16, as mentioned in Section 2.2, is that the volume ratio becomes the ratio between

the acoustic bulkling stiffness $K_a = \rho_0 c_0^2 S^2/V$ and the plate mass. The same conculsion was also shown in Ref. [11].

Figure A1 shows Ω and *D* as functions of the depth of the cavity (in *z*-direction, also the out-of-plane direction of the plate). Notice *D* is obtained from the plate velocity as in Eq. 18. The plate is simply supported and made of aluminum, with a dimension of 2.5 x 2 x 0.018 (m). It can be observed that the coupling strength undersoes fast decrease as the cavity depth increases, which is consistent with many previous researches [20, 25, 26]. Neverthless, the coupling strength is much weaker than that of an acoustic-acoustic system (typically one order of magnitude lower) even if the cavity is very shallow.

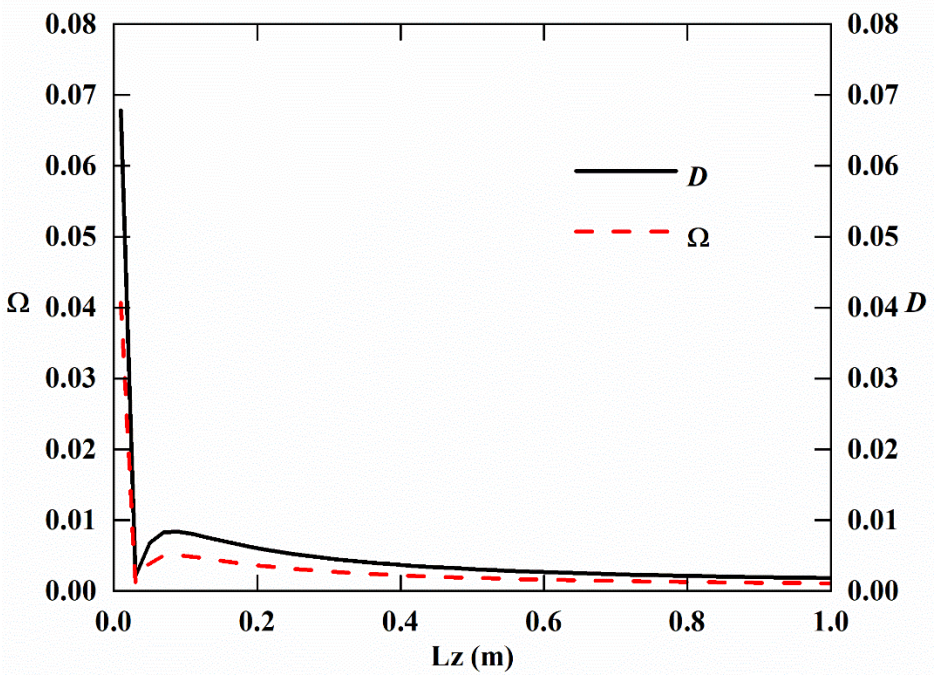

Figure A1 Effect of the cavity depth on the coupling strength of a plate-cavity system.

Reference

[1] M. Petyt, *Introduction to finite element vibration analysis*. 2010: Cambridge university press.

[2] P.K. Banerjee and R. Butterfield, *Boundary element methods in engineering science*. Vol. 17. 1981: McGraw-Hill London.

[3] Z.Y. Hu, L. Maxit, and L. Cheng, "Piecewise convergence behavior of the condensed transfer function approach for mid-to-high frequency modelling of a panel-cavity system," Journal of Sound and Vibration **435**(119-134 (2018).

[4] C. Soize, "A model and numerical method in the medium frequency range for vibroacoustic predictions using the theory of structural fuzzy," Journal of the Acoustical Society of America **94**(2), 849-865 (1993).

[5] R.S. Langley and P. Bremner, "A hybrid method for the vibration analysis of complex structural-acoustic systems," Journal of the Acoustical Society of America **105**(3), (1999).

[6] K. Vergote, B. Van Genechten, D. Vandepitte, and W. Desmet, "On the analysis of vibro-acoustic systems in the mid-frequency range using a hybrid deterministic-statistical approach," Computers & Structures **89**(11-12), 868-877 (2011).

[7] P.J. Shorter and R.S. Langley, "Vibro-acoustic analysis of complex systems," Journal of Sound and Vibration **288**(3), 669-699 (2005).

[8] R.R. Craig, "A review of time-domain and frequency-domain component mode synthesis method," Modal Analysis **2**(59-72 (1987).

[9] R.R. Craig, "Substructure methods in vibration," Journal of Vibration and Acoustics **117**(B), 207-213 (1995).

[10] M. Maess and L. Gaul, "Substructuring and model reduction of pipe components interacting with acoustic fluids," Mechanical systems and signal processing **20**(1), 45-64 (2006).

[11] S. Kim and M. Brennan, "A compact matrix formulation using the impedance and mobility approach for the analysis of structural-acoustic systems," Journal of Sound and Vibration **223**(1), 97-113 (1999).

[12] J.-D. Chazot and J.-L. Guyader, "Prediction of transmission loss of double panels with a patch-mobility method," Journal of the Acoustical Society of America **121**(1), 267-278 (2007).

[13] M. Ouisse, L. Maxit, C. Cacciolati, and J.-L. Guyader, "Patch transfer functions as a tool to couple linear acoustic problems," Journal of Vibration and Acoustics **127**(5), 458-466 (2005).

[14] V. Meyer, L. Maxit, J.L. Guyader, and T. Leissing, "Prediction of the vibroacoustic behavior of a submerged shell with non-axisymmetric internal substructures by a condensed transfer function method," Journal of Sound and Vibration **360**(260-276 (2016).

[15] S. De Rosa, F. Franco, X. Li, and T. Polito, "A similitude for structural acoustic enclosures," Mechanical Systems and Signal Processing **30**(330-342 (2012).

[16] L. Egab and X. Wang, "Objective evaluation of interior trim effects on sound quality and noise reduction of a coupled plate cavity system," Mechanical systems and signal processing **70**(919-931 (2016).

[17] S. Shi, Z. Su, G. Jin, and Z. Liu, "Vibro-acoustic modeling and analysis of a coupled acoustic system comprising a partially opened cavity coupled with a flexible plate," Mechanical Systems and Signal Processing **98**(324-343 (2018).

[18] X. Xie, H. Zheng, and Y. Qu, "A variational formulation for vibro-acoustic analysis of a panel backed by an irregularly-bounded cavity," Journal of Sound and Vibration **373**(147-163 (2016).

[19] Y. Chen, G. Jin, Z. Feng, and Z. Liu, "Modeling and vibro-acoustic analysis of elastically restrained panel backed by irregular sound space," Journal of Sound and Vibration **409**(201-216 (2017).

[20] E.H. Dowell, G.F. Gorman, and D.A. Smith, "Acoustoelasticity: General theory, acoustic natural modes and forced response to sinusoidal excitation, including comparisons with experiment," Journal of Sound and Vibration **52**(4), 519-542 (1977).

[21] P. Smith Jr, "Statistical models of coupled dynamical systems and the transition from weak to strong coupling," The Journal of the Acoustical Society of America **65**(3), 695-698 (1979).

[22] Y. Chen, G. Jin, and Z. Liu, "A domain decomposition method for analyzing a coupling between multiple acoustical spaces (L)," The Journal of the Acoustical Society of America **141**(5), 3018-3021 (2017).

[23] S. Shi, G. Jin, B. Xiao, and Z. Liu, "Acoustic modeling and eigenanalysis of coupled rooms with a transparent coupling aperture of variable size," Journal of Sound and Vibration **419**(352-366 (2018).

[24] Z. Hu, C. Yang, and L. Cheng, "Acoustic resonator tuning strategies for the narrowband noise control in an enclosure," Applied Acoustics **134**(88-96 (2018).

[25] F.J. Fahy, "Vibration of containing structures by sound in the contained fluid," Journal of Sound and Vibration **10**(3), 490-512 (1969).

[26] A.J. Pretlove, "Forced vibrations of a rectangular panel backed by a closed rectangular cavity," Journal of Sound and Vibration **3**(3), 252-261 (1966).